Electronic Supplementary Information

Nickel doped Lithium-vacant Layered $Li_yCr_{1-x}Ni_xO_2$: A Potentially Active Electrocatalyst for Oxygen Evolution Reaction

Vaishali Soni, [a] ***Shraddha Jaiswal,*** [a] ***Krishna Gopal Nigam,*** [b] ***Preetam Singh,*** [b] ***& Asha Gupta*** [a] *******

[a] *Department of Chemistry, Indian Institute of Technology (BHU), Varanasi-221005, India.*

[b] *Department of Ceramic Engineering, Indian Institute of Technology (BHU), Varanasi-221005, India.*

AUTHOR INFORMATION

***Corresponding Author:**

Email- asha.chy@itbhu.ac.in, toashagupta@gmail.com, Phone: +91 6390363140.

Electrochemical active surface area (ECSAs):

The ECSAs were determined by measuring the electrochemical double-layer capacitance (C_{dl}) in non-faradic potential regions of 0.9–0.1 V vs. Ag/AgCl at scan rates of 50, 70, 100, 120, 140, 160 mV s^{-1}. The C_{dl} values were calculated by plotting the current density differences (i_c= ΔJ/2) against scan rates (ν), where the slope represents C_{dl}, and given by the following equation:

$$i_c = C_{dl}\nu \ldots\ldots\ldots\ldots (Eq.1)$$

The ECSA of the catalysts was calculated by using the following formula:

$$ECSA = \frac{C_{dl}}{C_s} \ldots\ldots\ldots\ldots\ldots (Eq.2)$$

Where C_s is the specific capacitance of the material per unit area under identical electrolyte conditions. C_s = 0.040 mF cm^{-2} in 1.0 M KOH based on reported values [1].

Turnover frequency (TOF) calculation:

Turnover frequency of the synthesized catalysts was calculated at 350 mV overpotential based on the method reported in previous works [2]. This calculation assumes 100% Faradaic efficiency:

$$TOF = \frac{N_{O2}}{N_M} \ldots\ldots\ldots\ldots\ldots (Eq.3)$$

where N_{O2} is the number of O_2 turnovers, calculated using the following formula:

$$N_{O2} = j\left(mA\ cm^{-2}\right) \times \left(A\ cm^{2}_{oxide}\right) \times \left(\frac{1\ Cs^{-1}}{1000\ mA}\right) \times \left(\frac{1\ mol\ e^-}{96485\ C}\right) \times \left(\frac{1\ mol\ O_2}{4\ mol\ e^-}\right) \times N_A \ldots (Eq.4)$$

where, j is the measured current density at 350 mV overpotential, A is the surface area of carbon electrode (1 cm^2), and N_A is Avogadro constant (6.02 ×10^{23} mol^{-1}).

N_M is the number of active metal ions (Cr and Ni) for OER, which is calculated based on the mass loading of the samples (1 mg/cm^2) using the following formula:

- **For LCNO-0(c):** (ICP composition = $Li_{0.769}Cr_{1.003}O_2$)

$$N_M = (1.003Cr) \times \left(1 \times 10^{-3} g\right) \times \frac{N_A}{molecular\ weight}$$

$N_M = 0.0675 \times 10^{20}$

j = 11.74 mA cm^{-2} at 350 mV overpotential.

$$N_{O2} = 11.74\ \left(mA\ cm^{-2}\right) \times \left(1\ cm_{oxide}^{2}\right) \times \left(\frac{1\ Cs^{-1}}{1000\ mA}\right) \times \left(\frac{1\ mol\ e^-}{96485\ C}\right) \times \left(\frac{1\ mol\ O_2}{4\ mol\ e^-}\right) \times N_A$$

$$N_{O2} = 0.1831\ \times 10^{17}$$

$$TOF = \frac{0.1831 \times 10^{17}}{0.0676 \times 10^{20}} = 2.712 \times 10^{-3}\ s^{-1}$$

- **For LCNO-10(c):** (ICP composition = $Li_{0.698}Cr_{0.903}Ni_{0.098}O_2$)

$$N_M = (0.903Cr + 0.098Ni) \times \left(1 \times 10^{-3} g\right) \times \frac{N_A}{molecular\ weight}$$

$$N_M = 0.0674 \times 10^{20}$$

j = 40.6 mA cm^{-2} at 350 mV overpotential.

$$N_{O2} = 40.6\ \left(mA\ cm^{-2}\right) \times \left(1\ cm_{oxide}^{2}\right) \times \left(\frac{1\ Cs^{-1}}{1000\ mA}\right) \times \left(\frac{1\ mol\ e^-}{96485\ C}\right) \times \left(\frac{1\ mol\ O_2}{4\ mol\ e^-}\right) \times N_A$$

$$N_{O2} = 0.6334\ \times 10^{17}$$

$$TOF = \frac{0.6334 \times 10^{17}}{0.0674 \times 10^{20}} = 9.397 \times 10^{-3}\ s^{-1}$$

Determination of Faradaic Efficiency:

The faradaic efficiency of catalyst was determined by conducting the rotating ring-disk electrode (RRDE) experiment on an electrochemical work station based on Pine research

equipment (Wave Driver 200, USA). The experiment was performed using a rotating ring-disk electrode (RRDE) as working electrode that consists of a Pt ring and glassy carbon disk (0.196 cm^2), a Hg/HgO reference electrode and Pt wire counter electrode in 1 M KOH electrolyte. About 10 mg of LCNO-10(c) and 3 mg activated carbon were added in 1ml of water/isopropanol (3:1) solution containing 15 µl of Nafion binder, and dispersed by sonicating for 30 min to generate homogenous catalyst ink. About 10 µl of catalyst ink was coated onto the GC disk (RRDE) with a catalyst loading amount of ~0.5 mg cm^{-2}. An LSV curve was recorded at a scan rate of 5 mV s^{-1} with a rotation rate of 1400 rpm by sweeping the potential at the disk from 1.0 to 1.8 V vs. RHE, and the O_2 molecules that evolved were reduced at the Pt ring, where a potential of −0.5 V was kept constant to enable an efficient oxygen reduction reaction (ORR). The calculation of the faradaic efficiency was performed using the following equation [3]:

$$Faradaic\ Efficiency = \frac{j_R \times n_D}{j_R \times n_R \times N_{CL}} \ldots\ldots\ldots\ldots (Eq.5)$$

where, j_R and j_D are the ring and disk current densities at a particular potential, n_D and n_R are the number of electrons transferred during the evolution and reduction of O_2 at disk and ring, respectively, which is 4. N_{CL} is the collection efficiency of the RRD electrode. The average collection efficiency of the RRDE used here is 0.439.

For LCNO-10(c): at 1.6 V vs. RHE

$$\textbf{FE} = 13.2 \times 4 / 32.9 \times 4 \times 0.439$$

$$= 0.9139 \times 100$$

$$= 91.39\ \%$$

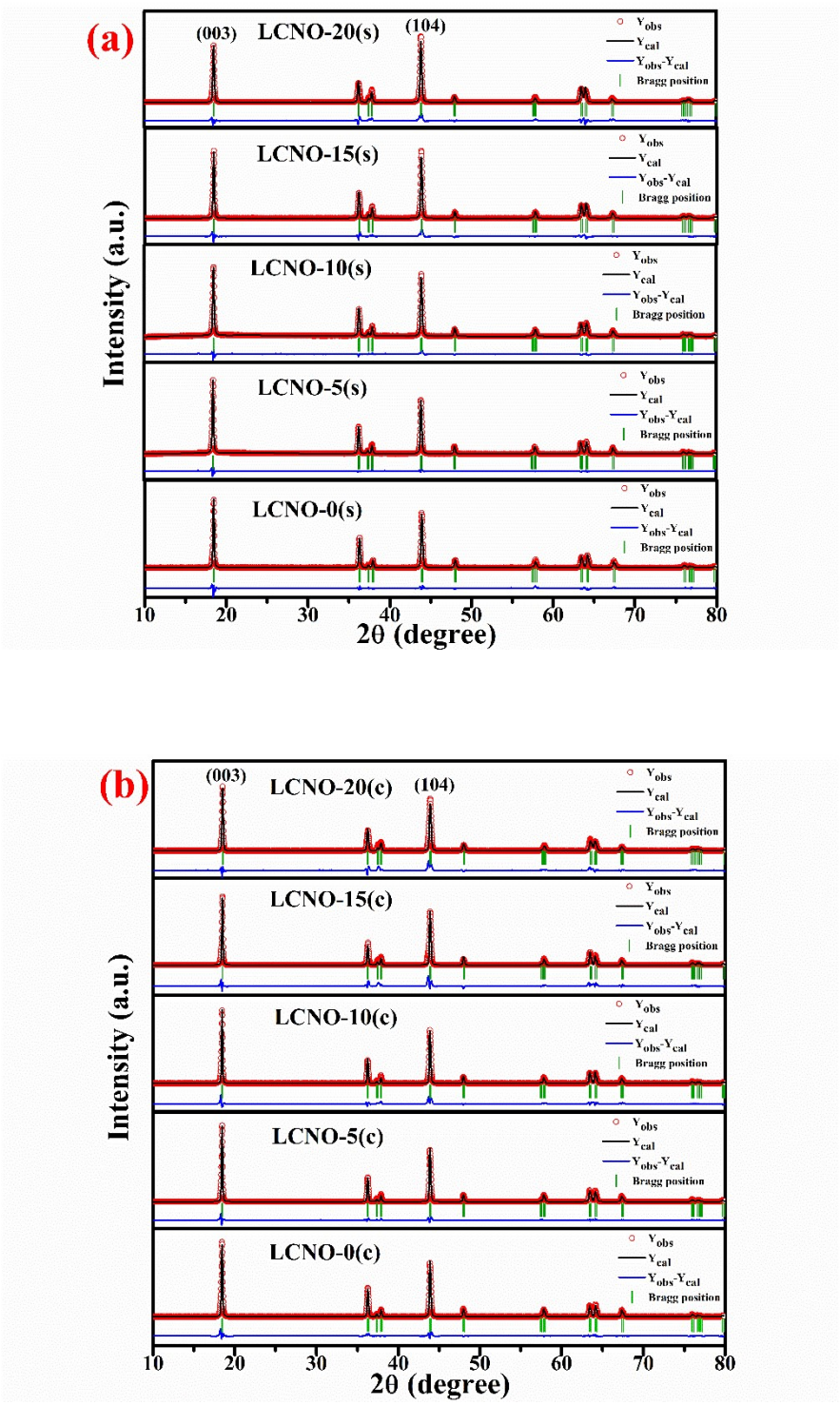

Fig. S1 Rietveld refined powder XRD patterns of $Li_yCr_{1-x}Ni_xO_2$ ($y \leq 1$, $0 \leq x \leq 0.2$). **(a)** solid-state and **(b)** solution combustion synthesized samples.

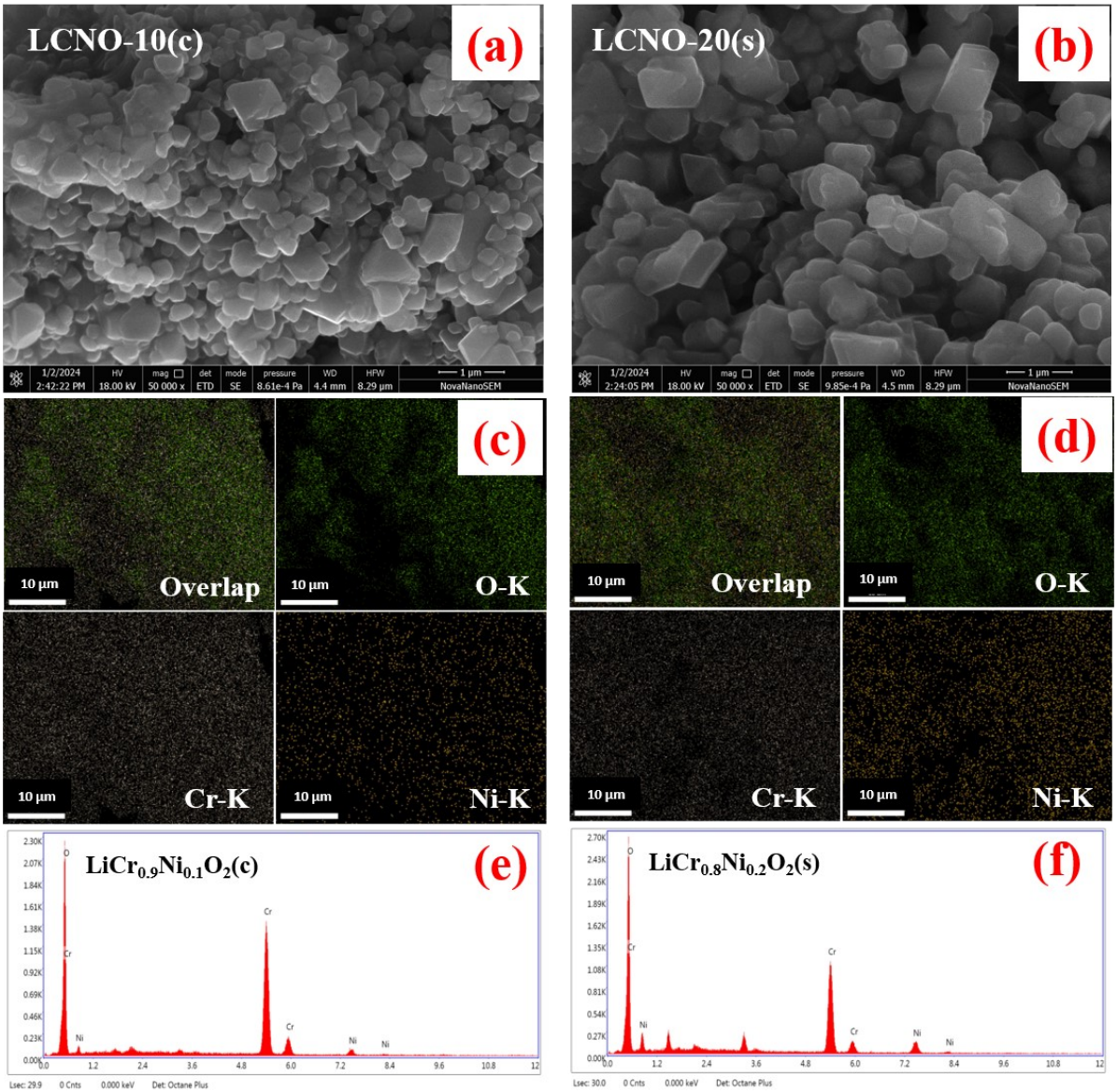

Fig. S2 SEM micrograph of **(a)** LCNO-10(c), **(b)** LCNO-20(s), **(c), (d)** elemental mapping of individual elements (O, Cr, and Ni) present in the LCNO-10(c) and LCNO-20(s) samples, respectively, and **(e), (f)** EDS spectrum of LCNO-10(c) and LCNO-20(s). Note: Li signals are absent in EDS analysis as EDS techniques are not capable of recording signals for the Li core level.

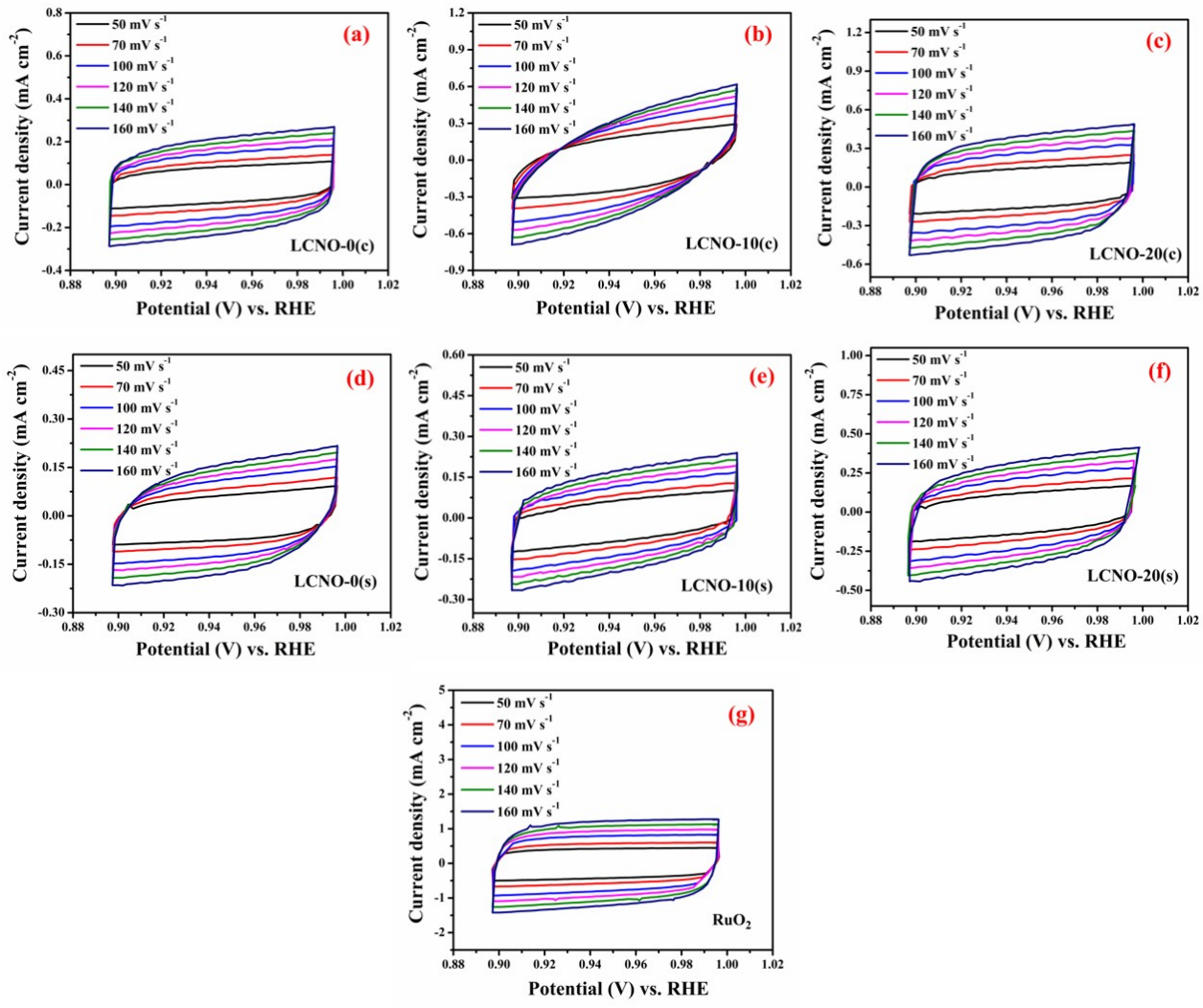

Fig. S3 Determination of double layer capacitance (C_{dl}) of different LCNOs (synthesized by solid-state and combustion method) and commercial RuO_2. **(a-g)** CV measurements in a non-faradic current region (0.9-1.0 V vs. RHE) at scan rates of 50, 100, 120, 140 and 160 mV s^{-1}in 1 M KOH electrolyte.

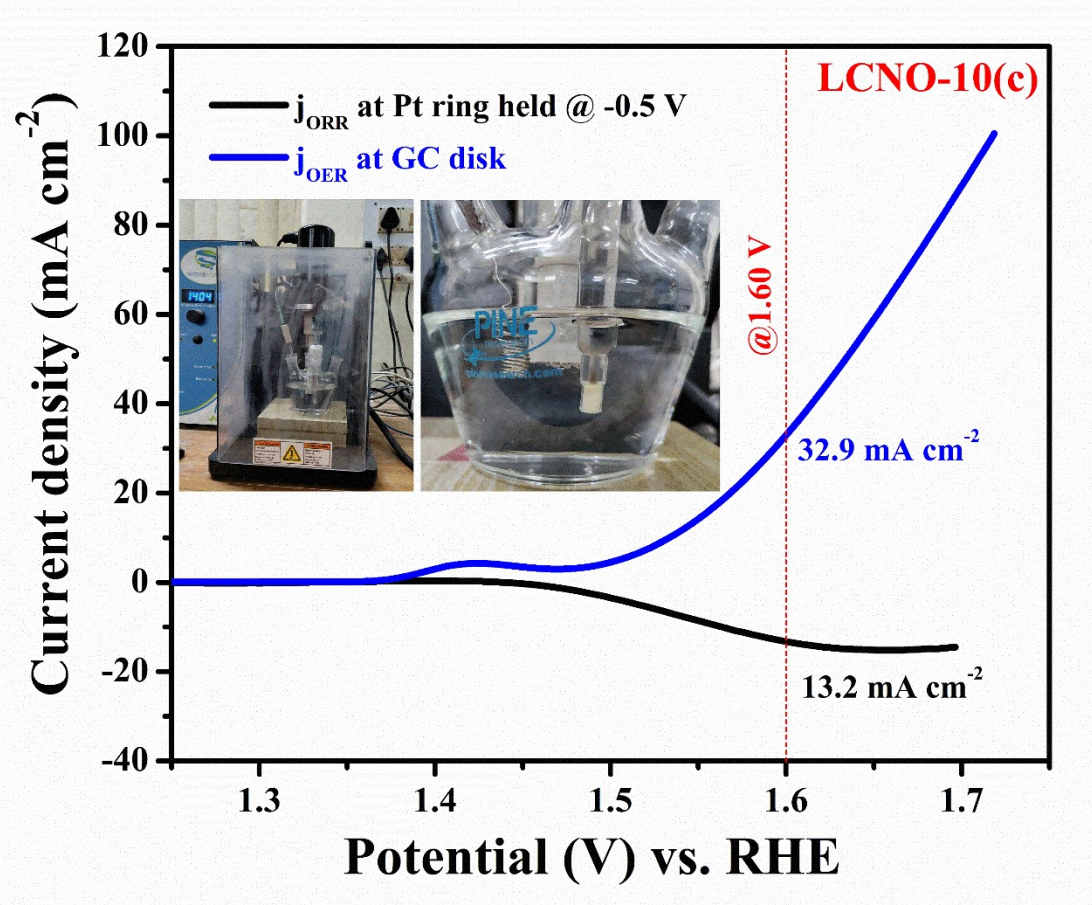

Fig. S4 The RRDE polarization at GC disk and the corresponding ORR response at Pt ring obtained with LCNO-10(c) for faradaic efficiency calculation.

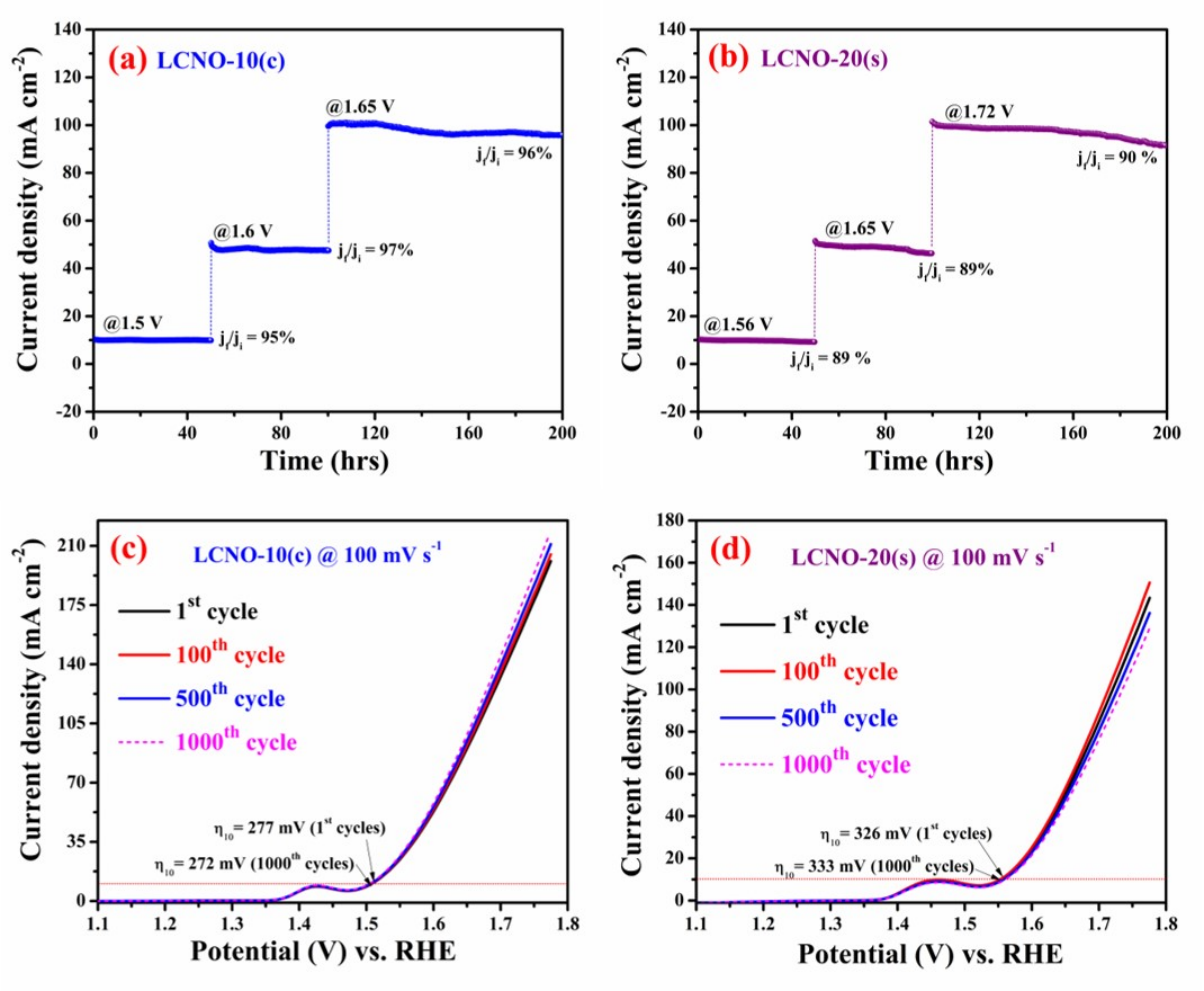

Fig. S5 Stability test **(a)** chronoamperogram of LCNO-10(c) at measured potential of 1.5, 1.6 and 165 V vs. RHE for 200 hrs, **(b)** chronoamperogram of LCNO-20(s) at measured potential of 1.56, 1.65 and 1.72 V vs. RHE for 200 hrs, and **(c), (d)** shows the linear sweep voltammograms for the 1st, 100th, 500th and 1000th cycle at a scan rate of 100 mV s^{-1}. (Note: the long-term chronoamperometry test was performed using Hg/HgO reference electrode).

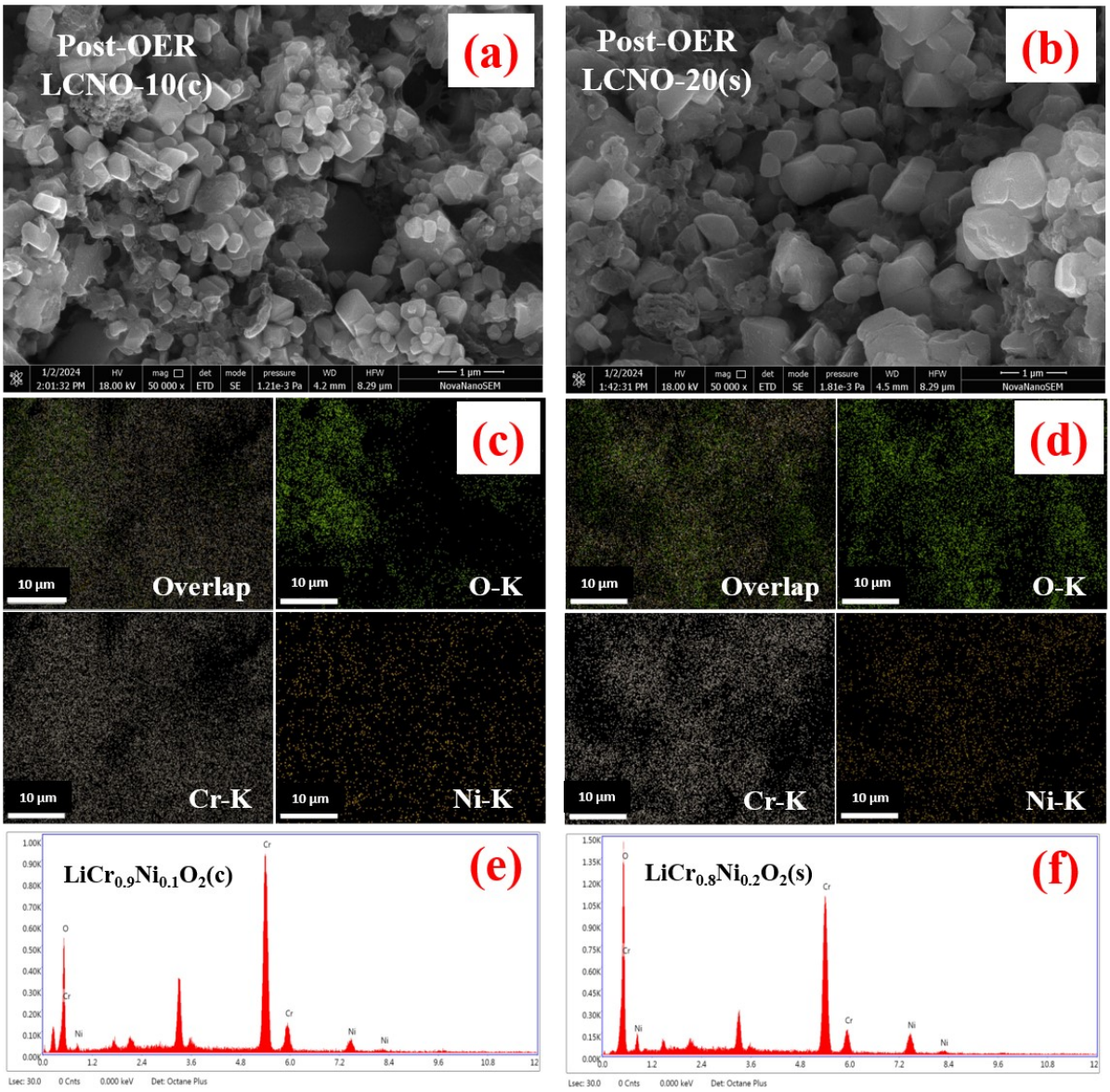

Fig. S6 Post-OER SEM micrographs of **(a)** LCNO-10(c), **(b)** LCNO-20(s), **(c), (d)** corresponding elemental mapping and **(e), (f)** EDS spectrum confirming the presence of O, Cr, and Ni in the LCNO-10(c) and LCNO-20(s) electrodes, respectively. Note: Li signals are absent in EDS analysis as EDS techniques are not capable of recording signals for the Li core level.

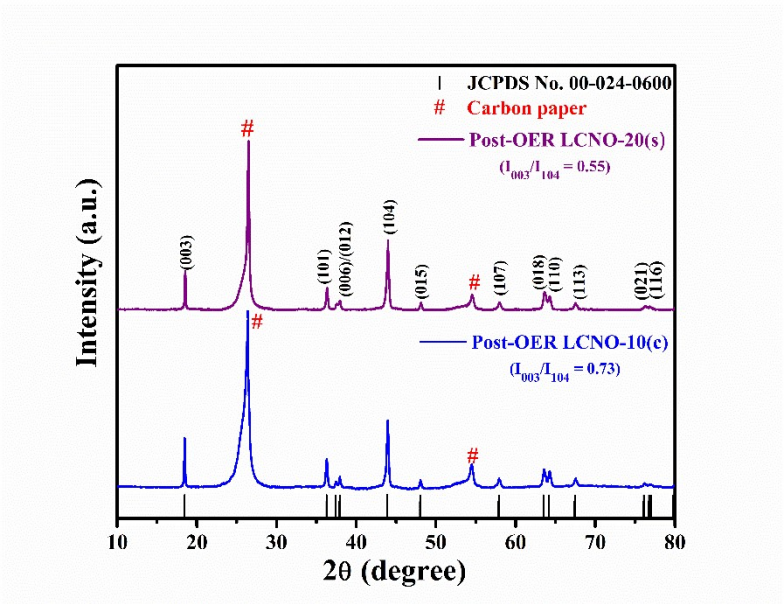

Figure S7 Post-OER XRD pattern of LCNO-10(c) and LCNO-20(s) electrodes.

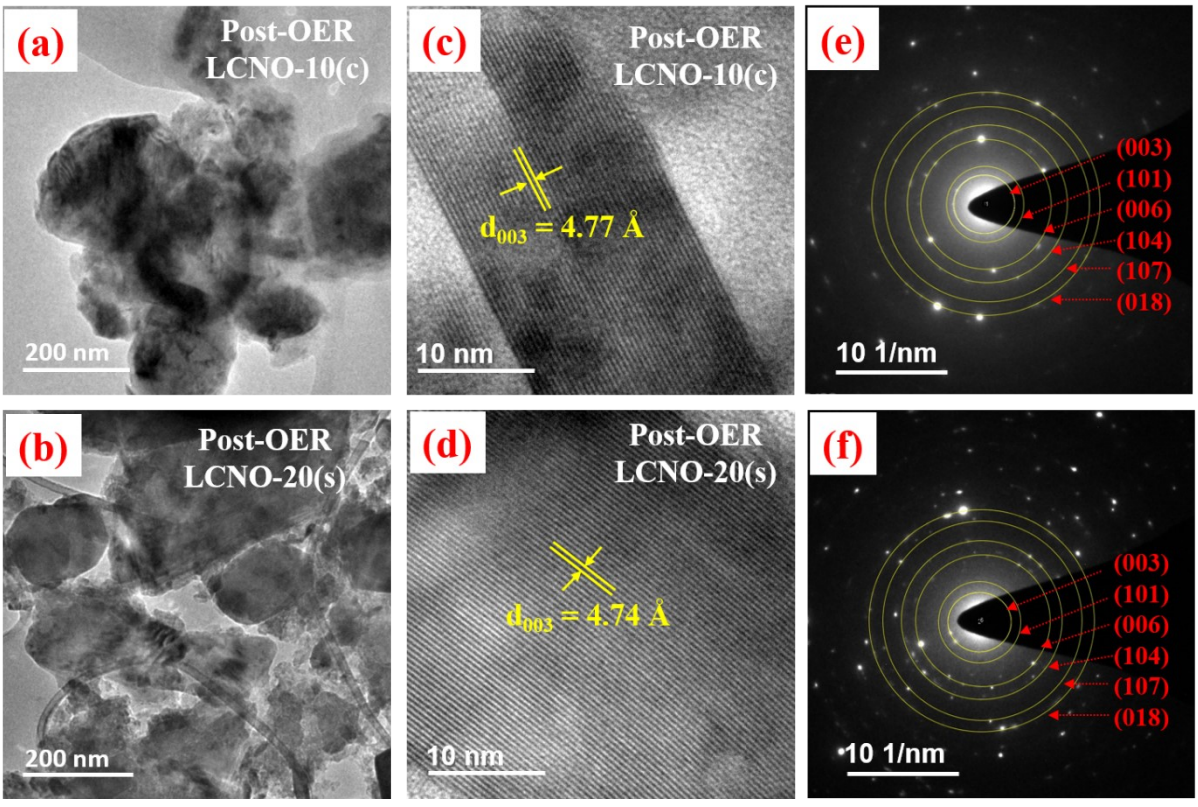

Fig. S8 Post-OER TEM micrographs. **(a), (b)** Bright-field TEM image, **(c), (d)** HR-TEM with interplanar d-spacing of (003) plane, **(e), (f)** SAED pattern of LCNO-10(c) and LCNO-20(s) samples, respectively.

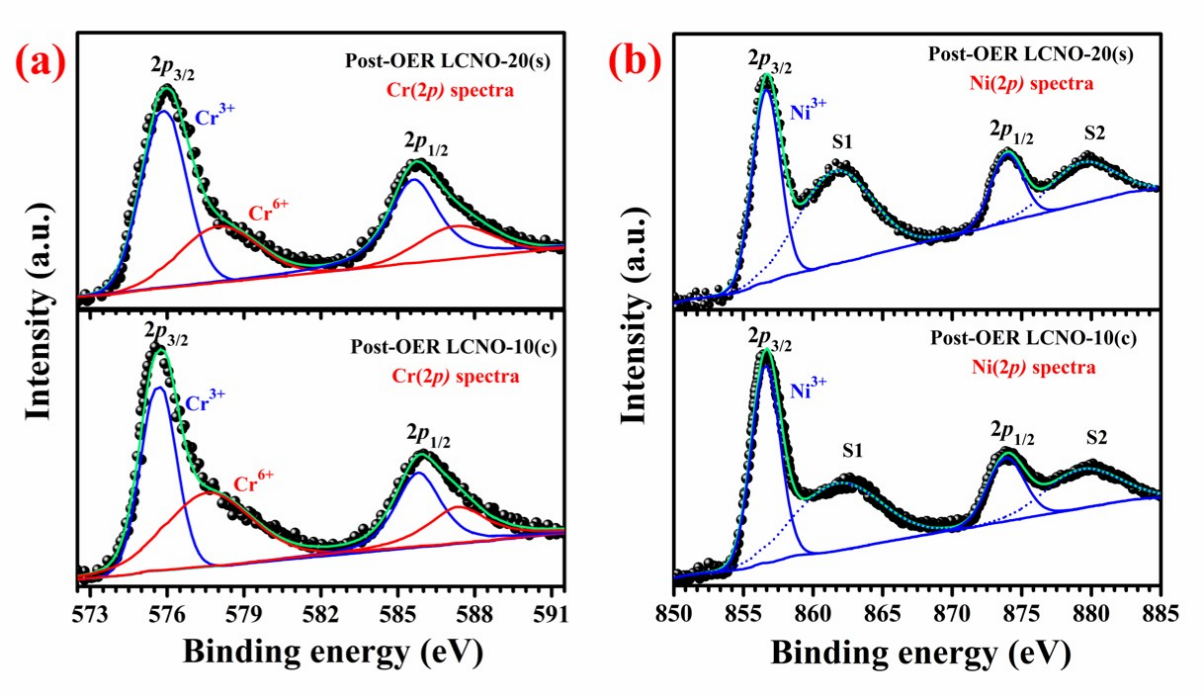

Fig. S9 Post-OER **(a)** Cr(2*p*) and **(b)** Ni(2*p*) spectra of LCNO-10(c) and LCNO-20(s) electrodes.

Table S1. XPS deconvoluted peak positions and % composition in Cr(2*p*) spectra for $Li_yCr_{1-x}Ni_xO_2$ ($y \leq 1$, $0 \leq x \leq 0.2$) synthesized by combustion and solid-state method.

Samples			Binding energy (eV)		Relative concentration (%)
			$2p_{3/2}$	$2p_{1/2}$	
Solid state method	LCNO-0(s)	Cr^{3+}	575.3	585.4	89
		Cr^{6+}	577.5	587.4	11
	LCNO-10(s)	Cr^{3+}	575.7	585.6	81
		Cr^{6+}	577.6	587.6	19
	LCNO-20(s)	Cr^{3+}	575.8	585.8	74
		Cr^{6+}	577.7	587.7	26
Combustion method	LCNO-0(c)	Cr^{3+}	575.6	585.3	86
		Cr^{6+}	577.5	587.2	14
	LCNO-10(c)	Cr^{3+}	575.9	585.7	67
		Cr^{6+}	577.4	587.3	33
	LCNO-20(c)	Cr^{3+}	575.7	585.5	71
		Cr^{6+}	577.4	587.4	29

Table S2. XPS deconvoluted peak positions and % composition in Ni(2*p*) spectra for $Li_yCr_{1-x}Ni_xO_2$ ($y \leq 1$, $0 \leq x \leq 0.2$) synthesized by combustion and solid-state method.

Samples			Binding energy (eV)				Relative concentration (%)
			$2p_{3/2}$	$2p_{1/2}$	S1	S2	
Solid state method	LCNO-10(s)	Ni^{3+}	855.3	873.1	861.4	878.9	76
		Ni^{2+}	853.6	871.4	859.3	877.0	24
	LCNO-20(s)	Ni^{3+}	855.4	873.3	861.1	879.0	81
		Ni^{2+}	853.8	871.3	859.4	877.1	19
Combustion method	LCNO-10(c)	Ni^{3+}	855.5	873.3	861.2	879.2	90
		Ni^{2+}	853.9	871.6	859.2	877.1	10
	LCNO-20(c)	Ni^{3+}	855.4	873.4	861.1	879.1	85
		Ni^{2+}	853.7	871.5	859.3	877.2	15

Table S3. The fitted R_{ct} values from the Nyquist plot for $Li_yCr_{1-x}Ni_xO_2$ ($y \leq 1$, $0 \leq x \leq 0.2$) catalysts synthesized by combustion and solid-state method.

Solid-state synthesized samples (s)	R_{ct} (Ω)	Combustion synthesized samples (c)	R_{ct} (Ω)
LCNO-0(s)	37.03	LCNO-0(c)	19.25
LCNO-5(s)	23.66	LCNO-5(c)	14.65
LCNO-10(s)	20.43	LCNO-10(c)	6.6
LCNO-15(s)	16.24	LCNO-15(c)	8.85
LCNO-20(s)	11.36	LCNO-20(c)	12.3

Table S4. Tafel slope and R_{ct} values of synthesized catalysts along with commercial RuO_2 (as a benchmark catalyst).

Catalysts	Tafel slope (mV dec^{-1})	R_{ct} (Ω)
RuO_2	83	17.33
LCNO-10(c)	63	6.6
LCNO-20(c)	79	12.3
LCNO-10(s)	85	20.43
LCNO-20(s)	95	11.36

Table S5. Calculated C_{dl} and ECSA values for $Li_yCr_{1-x}Ni_xO_2$ ($y \leq 1$, $0 \leq x \leq 0.2$) catalysts synthesized by combustion and solid-state method along with commercial RuO_2 (as a benchmark catalyst).

Catalyst	C_{dl} (mF cm^{-2})	ECSA (cm^2 mg^{-1})
LCNO-0(c)	1.53	38.25
LCNO-10(c)	3.2	80
LCNO-20(c)	2.8	70
LCNO-0(s)	1.13	28.25
LCNO-10(s)	1.3	32.5
LCNO-20(s)	2.3	57.5
RuO_2	7.9	197.5

Table S6: Turnover frequencies (TOF) of different $Li_yCr_{1-x}Ni_xO_2$ ($y \leq 1$, $0 \leq x \leq 0.2$) catalysts synthesized by combustion and solid-state method.

Samples		ICP composition	No. of O_2 turnover (N_{O2})	No. of active metal ions (N_M)	TOF (s^{-1})
Combustion method	**LCNO-0(c)**	$Li_{0.769}Cr_{1.003}O_2$	0.1831×10^{17}	0.0675×10^{20}	2.71×10^{-3}
	LCNO-5(c)	$Li_{0.799}Cr_{0.949}Ni_{0.049}O_2$	0.2802×10^{17}	0.0669×10^{20}	4.19×10^{-3}
	LCNO-10(c)	$\mathbf{Li_{0.698}Cr_{0.903}Ni_{0.098}O_2}$	$\mathbf{0.6334\times10^{17}}$	$\mathbf{0.0674\times10^{20}}$	$\mathbf{9.39\times10^{-3}}$
	LCNO-15(c)	$Li_{0.778}Cr_{0.851}Ni_{0.148}O_2$	0.4725×10^{17}	0.0666×10^{20}	7.09×10^{-3}
	LCNO-20(c)	$Li_{0.749}Cr_{0.801}Ni_{0.199}O_2$	0.3929×10^{17}	0.0665×10^{20}	5.91×10^{-3}
Solid-state method	**LCNO-0(s)**	$Li_{0.669}Cr_{1.003}O_2$	0.0659×10^{17}	0.0679×10^{20}	0.98×10^{-3}
	LCNO-5(s)	$Li_{0.749}Cr_{0.949}Ni_{0.051}O_2$	0.1635×10^{17}	0.0672×10^{20}	2.43×10^{-3}
	LCNO-10(s)	$Li_{0.731}Cr_{0.902}Ni_{0.098}O_2$	0.1527×10^{17}	0.0671×10^{20}	2.27×10^{-3}
	LCNO-15(s)	$Li_{0.720}Cr_{0.851}Ni_{0.149}O_2$	0.2193×10^{17}	0.0668×10^{20}	3.28×10^{-3}
	LCNO-20(s)	$Li_{0.698}Cr_{0.801}Ni_{0.198}O_2$	0.2608×10^{17}	0.0667×10^{20}	3.91×10^{-3}

Table S7. The post-OER ICP analysis of $Li_yCr_{1-x}Ni_xO_2$ ($y \leq 1$, $0 \leq x \leq 0.2$) synthesized by combustion and solid-state method.

Samples		Post-OER ICP composition of $Li_yCr_{1-x}Ni_xO_2$ ($y \leq 1$, $0 \leq x \leq 0.2$)		
		Li	**Cr**	**Ni**
Combustion method	**LCNO-0(c)**	0.767	1.001	0.000
	LCNO-5(c)	0.798	0.948	0.048
	LCNO-10(c)	0.696	0.899	0.097
	LCNO-15(c)	0.775	0.848	0.147
	LCNO-20(c)	0.745	0.799	0.198
Solid-state method	**LCNO-0(s)**	0.668	1.003	0.000
	LCNO-5(s)	0.748	0.947	0.049
	LCNO-10(s)	0.718	0.897	0.097
	LCNO-15(s)	0.729	0.849	0.148
	LCNO-20(s)	0.695	0.797	0.198

References:

1. C. C. L. McCrory, S. Jung, I. M. Ferrer, S. M. Chatman, J. C. Peters and T. F. Jaramillo, Benchmarking hydrogen evolving reaction and oxygen evolving reaction electrocatalysts for solar water splitting devices, *J. Am. Chem. Soc*., 2015, **137**(13), 4347–4357.
2. Y. Lin, Z. Tian, L. Zhang, J. Ma, Z. Jiang, B. J. Deibert, R. Ge and L. Chen, Chromium-ruthenium oxide solid solution electrocatalyst for highly efficient oxygen evolution reaction in acidic media, *Nature Commun.,* 2019, **10**(1), 162.
3. S. Anantharaj, P. E. Karthik and S. Kundu, Petal-like hierarchical array of ultrathin $Ni(OH)_2$ nanosheets decorated with $Ni(OH)_2$ nanoburls: a highly efficient OER electrocatalyst, *Catal. Sci. Technol.*, 2017, **7**, 882-893.